ACS Sustainable Chemistry & Engineering
pubs.acs.org/journal/ascecg
Research Article

Understanding the Thermal Behavior of Black Mass during Recycling of Spent Lithium-Ion Batteries through Its Individual Components

Moses Charles Siame,* Hesham M. Ahmed, Anton Andersson, and Lena Sundqvist-Öqvist

Cite This: https://doi.org/10.1021/acssuschemeng.5c10344
Read Online
ACCESS | Metrics & More | Article Recommendations

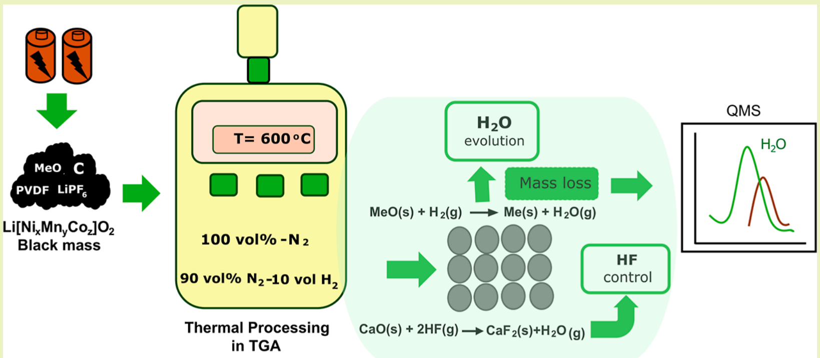

ABSTRACT: The increasing use of lithium-ion batteries (LiBs) in electric vehicles and electronics has made efficient recycling essential for maintaining a reliable and affordable supply of critical metals. Thermal treatment of black mass (BM), the heterogeneous residue from spent LiBs, is a crucial step to improve downstream material separation and recovery. This study investigates the thermal behavior of LiBs BM by analyzing the thermal behavior of its components when heated to 600 °C in an inert (N_2) atmosphere or in a mixture of 90 vol % N_2 and 10 vol % H_2. Thermogravimetric analysis (TGA) was conducted at a heating rate of 10 °C/min with an isothermal hold of 1 h, and coupled with quadrupole mass spectrometry (QMS). The analysis was performed on graphite, activated carbon, lithium hexafluorophosphate ($LiPF_6$), polyvinylidene fluoride (PVDF), synthetic black mass, and lithium nickel manganese cobalt oxide (NMC) industrial BM. Equilibrium calculations conducted in FactSage 8.3 were used to describe and understand the experimental findings. The TGA results indicate that in 100 vol % N_2, graphite exhibited the lowest weight loss of 0.1 wt %, followed by activated carbon at 2.9 wt %, PVDF at 56 wt %, and $LiPF_6$ at 81 wt %. Synthetic black mass had a weight loss of 3.4 wt %, while industrial black mass had 1.0 wt %. In 90 vol % N_2/10 vol % H_2, $LiPF_6$ and PVDF experienced weight losses of 79 and 64 wt %, respectively. Synthetic BM had a weight loss of 15.1 wt %, and industrial BM 15.6 wt % due to enhanced reduction of metal oxides in the presence of hydrogen.

KEYWORDS: *spent lithium-ion batteries, sustainable recycling, pretreatment, thermal decomposition, hydrogen-assisted reduction*

1. INTRODUCTION

The global transition to clean energy and sustainable technologies has led to an increased demand for lithium-ion batteries (LiBs), which is driven by the rapid growth of the electric vehicle (EV) market and the need for efficient energy storage.[1] LiBs offer many advantages, such as high energy density and a lightweight design, making them ideal for powering EVs, electronics, and various modern technologies. However, the rapid increase in their usage has also led to a rise in battery waste. Spent LiBs can pose significant environmental risks due to the presence of toxic and flammable materials. Furthermore, if not adequately managed or recycled, LiBs can create safety hazards, including fires, explosions, and chemical leaks.[2] Recycling of LiBs is a sustainable approach that recovers valuable materials and reduces dependence on primary raw material extraction. An essential stage in spent LiBs recycling is the mechanical processing, which involves shredding, crushing, and physical separation techniques.[3] This mechanical processing generates various materials, including casings and plastics. The fine material left after physical separation is called black mass (BM), which contains a concentrated fraction of anode

Received: September 24, 2025
Revised: December 12, 2025
Accepted: December 18, 2025

and cathode materials along with residual organic binders, traces of electrolytes, fragments of current collectors such as aluminum (Al) foil from cathodes and copper (Cu) foil from anodes, remnants of plastic-based separators,[4] and electrolyte lithium hexafluorophosphate ($LiPF_6$), which is a salt dissolved in organic solvents such as ethylene carbonate (EC) and diethyl carbonate (DEC).[5,6] A common binder used in LiBs is the polyvinylidene fluoride (PVDF), which is known for its chemical stability and strong adhesion in electrode fabrication.[7] However, during the pyrometallurgical recycling of lithium-ion batteries (LiBs), both $LiPF_6$ and PVDF thermally decompose, resulting in the release of hazardous fluorine-containing gases, such as hydrogen fluoride (HF), along with other volatile fluorinated compounds.[8]

The electrolyte $LiPF_6$ exhibits thermal stability up to 107 °C in dry conditions, where the moisture content is maintained below 10 ppm in an inert atmosphere. Beyond this temperature, the decomposition of $LiPF_6$ results in the formation of lithium fluoride (LiF) as a solid and gaseous phosphorus pentafluoride (PF_5).[9] Previous studies[9,10] have indicated that secondary reactions occur in the presence of water vapor, where PF_5 gas, produced during the decomposition of $LiPF_6$, interacts with moisture to form compounds such as POF_3.[10] Additionally, the presence of moisture lowers the decomposition onset temperature, releasing fluorine-containing gases such as PF_5, POF_3, and HF.[11]

PVDF undergoes thermal degradation at approximately 350 °C through a multistep decomposition reaction, which is strongly influenced by conditions such as reaction temperature, atmosphere, and the presence of reactive additives like calcium oxide (CaO).[12] The type of atmosphere, whether inert, reducing, or oxidizing, determines the types and amounts of gases that are released during degradation.[13,14] The primary degradation mechanism under inert conditions involves the breaking of carbon−fluorine (C−F) and carbon−hydrogen (C−H) bonds, leading to the release of HF and a range of hydrocarbon species, including aliphatic and olefinic compounds.[15,16] When $LiPF_6$ and PVDF are part of the BM, the thermal behavior of the BM is affected by how these components behave and interact with other components, such as the active cathode and anode materials, as well as any residual solvents. The presence of transitional metal oxides, such as NiO or CoO, in lithium nickel manganese cobalt oxide (NMC) cathodes also influences the degradation mechanism of polymers,[17] potentially affecting how $LiPF_6$ and PVDF decompose in the BM. Another component of LiBs' BM, which influences their thermal behavior, is aluminum (Al), which serves as the current collector onto which the cathode material is coated. When BM containing Al is heated, Al reacts with Li or fluorine species, which may produce compounds such as lithium aluminum oxide ($LiAlO_2$) or aluminum fluoride (AlF_3).[18] Recent studies have reported that cobalt (Co) in BM containing lithium cobalt oxide ($LiCoO_2$) can be reduced by Al when heated at a temperature of 600 °C in an argon atmosphere.[19] Essentially, at 600 and 700 °C, both carbon (from graphite) and Al contribute to the decomposition of the cathode active material ($LiNi_xMn_yCo_zO_2$). Specifically, carbon facilitates a carbothermic reduction, reacting with metal oxides in $LiCoO_2$ to form elemental metals and carbon oxides,[19,20] while Al results in an aluminothermic reduction, where it reduces metal oxides to form alumina (Al_2O_3) and elemental metals. In the case of NMC batteries, it is reported that carbothemic reduction at a temperature of 650 °C promotes the decomposition of the cathode active material by reducing the oxides of Co, Ni, and Mn to lower oxidation states.[20] Other studies have also reported that pure graphite and NMC mixtures do not exhibit mass loss when heated in isolation up to 720 °C in inert gas environments.[21] Studies indicate that LiBs materials containing NMC cathode material mixed with carbon black or coke, when heated in an argon atmosphere in a TG/DSC,[22,23] exhibit an exothermic response between 550 and 700 °C followed by the initial stages of reduction of nickel and cobalt oxides.[21−24]

The thermal behavior of LiBs' BM is fundamentally driven by the composition of components and the temperature range in which each component degrades, interacts, and transforms. While previous studies have provided general insights into the degradation mechanism of LiBs' BM, further research is needed to clarify how specific BM constituents influence its thermal behavior under varying recycling conditions. The present study investigates how interactions between BM constituents affect the thermal behavior of BM at temperatures up to 600 °C under an inert atmosphere and a 10 vol % H_2 added atmosphere, the latter simulates the reducing atmosphere conditions that can be beneficial at lower temperatures, to promote selective reduction of metal oxides in BM and enhance metal recovery in subsequent processing stages. The thermal characteristics of individual active materials used in LiBs production are analyzed to determine their specific contributions to the overall thermal behavior of BM. Additionally, the thermal behavior of synthetic black, prepared from those materials, is investigated to identify the trends observed in industrial black mass samples. The study also explains the behavior of fluorine during the thermal treatment of LiBs black mass. By separately analyzing the fluorine-containing components, such as the PVDF and $LiPF_6$, and then examining their combined behavior with other LiBs components, it reveals how individual constituents interact to govern fluorine release from the black mass. Further, the study identifies that the presence of Ca and Al in black mass can effectively retain fluorine by forming stable fluoride compounds, which greatly reduces HF release during thermal treatment of industrial black mass. The study integrates thermogravimetric analysis coupled with quadrupole mass spectrometry (TGA-QMS) and thermodynamic modeling under both inert and reducing atmospheres to identify the formation pathways of HF, CH_4, and CO_2 through a combination of equilibrium predictions and experimental gas evolution measurements. It also reveals how hydrogen-containing atmospheres influence the reduction of Ni and Co oxides at lower temperatures. The study therefore provides essential knowledge needed to design safer, more controlled, and more efficient thermal pretreatment processes for Li-ion battery recycling, supporting the development of more sustainable and environmentally responsible recycling practices.

2. MATERIALS AND METHODS

2.1. Preparation of Synthetic Black Mass. The chemicals used to prepare the synthetic black mass samples were powders of lithium nickel manganese cobalt oxide ($LiNiCoMnO_2$-NMC 811, MTI), lithium hexafluorophosphate ($LiPF_6$, 98 wt %, Thermo Scientific), polyvinylidene fluoride binder ($[C_2H_2F_2]_n$, MTI), conductive graphite (C, 99.9 wt %, MTI) and activated carbon (C, 99.8 wt %, Thermo Scientific). The synthetic black mass was prepared by blending 70 wt % of NMC 811 powder with 25 wt % graphite, 3 wt % activated carbon, 1 wt % PVDF binder, and 1 wt % $LiPF_6$. The powders were

https://doi.org/10.1021/acssuschemeng.5c10344
ACS Sustainable Chem. Eng. XXXX, XXX, XXX−XXX

thoroughly homogenized in an agate mortar to ensure uniform mixing and minimize agglomeration. No additional binder or compaction step was applied. The mixing of these powders was done in a glovebox under an Ar atmosphere with an O_2 level of less than 1 ppm.

2.2. Characterization of the Black Mass. The BM samples supplied by a company were generated from a mixture of lithium-ion batteries. The samples were analyzed using inductively coupled plasma optical emission spectroscopy (ICP−OES) to quantify the concentrations of Li, Ni, Co, Mn, Cu, and Al. Before the ICP−OES analysis, the black mass sample was dissolved in aqua regia at 100 °C for 1 h and diluted 2000 times with a 2 vol % HNO_3 solution. The analysis was performed using a ThermoScientific iCAP 7200 ICP-OES instrument.

The carbon content in the BM sample was determined through combustion analysis using an elemental analyzer (Eurovector EA3000) in which the sample was heated in a combustion chamber to 1000 °C in the presence of oxygen gas (O_2), ensuring complete oxidation of all carbon-based compounds to carbon dioxide (CO_2). The produced CO_2 was measured using an infrared (IR) detector that detects absorption of infrared light at specific wavelengths associated with CO_2. The amount of CO_2 detected is directly related to the carbon content in the sample. To ensure precise measurements, the detector was calibrated with established standards, and the resulting data were evaluated to calculate the percentage of carbon in the black mass samples.

The amount of F contained in the black mass was determined using the ion-selective electrode (ISE) 9214 method.[25] The method involves fusing the samples with sodium peroxide (Na_2O_2) at 800 °C. The resulting melt was dissolved in hot water, diluted and pH-adjusted before being mixed with a total ionic strength adjustment buffer (TISAB) to stabilize the electric potential and mask specific interfering ions. Calibration was performed by recording the potential values (in millivolts, mV) of the ion-selective electrode (ISE) for standard fluoride solutions at different concentrations. The amount of fluorine in BM was calculated by comparing the potential readings in millivolts to the calibration curve.

The phase composition of the black mass was analyzed using a Malvern Panalytical Empyrean X-ray diffractometer (XRD) (Malvern, UK) using Cu-Kα radiation. The instrument operated at 40 mA and 45 kV. Diffraction patterns were recorded over a 2θ range of 10° to 90° with a scanning step size of 0.026° and a scan time of 87.5 s per step. Phase identification was conducted using HighScore Plus software, with references from the Crystallography Open Database (COD).[26]

2.3. Thermodynamic Calculations. Thermodynamic equilibrium calculations for PVDF, $LiPF_6$, synthetic black mass and original black mass were conducted using the Equilib module in FactSage 8.3 to understand their behavior under experimental conditions. The simulations considered all possible stoichiometric solid and gas phases by using the FactPS database.[27] Additionally, the FTsalt database was included explicitly for $LiPF_6$. For the input conditions, 1 g of each sample was assumed, with an atmosphere of 1.6×10^{-3} m^3 N_2 per gram of the samples representing 100 vol % pure N_2, or an atmosphere composed of 1.44×10^{-3} m^3 N_2 and 1.6×10^{-4} m^3 H_2 per gram of the samples, representing a gas mixture of 90 vol % N_2 and 10 vol % H_2. The monomer 1,2-difluoroethane ($C_2H_2F_2$) was used to simulate the PVDF binder. The monomer $C_2H_2F_2$ represented an idealized approximation of the elemental composition of the polymer and is widely used in equilibrium modeling of polymer-containing systems. While it does not explicitly describe the polymer chain structure or degradation kinetics, it sufficiently captures the overall thermodynamic behavior and elemental interactions relevant to PVDF decomposition under the studied conditions.

2.4. Thermogravimetric and Gas Emission Analysis. Thermogravimetric analysis (TGA) was conducted using a Netzsch STA 409 with a detection limit of ±1 μg to investigate the thermal behavior of black mass, graphite, activated carbon, electrolyte, cathode powder, synthetic BM, and industrial BM. Samples were heated at 10 °C/min to 600 °C and held at this temperature for 1 h under a N_2 gas flow of 100 mL/min. In another set of tests, all the samples were subjected to the same thermal conditions but in a gas mixture of 90 vol % N_2 and 10 vol % H_2. The goal was to assess how a mixed gas atmosphere influences the thermal behavior of the LiBs components. Off-gases released during the tests were ionised and qualitatively analyzed using a quadrupole mass spectrometer (QMS).

3. RESULTS

3.1. Material Characterization. Table 1 presents the composition of the synthetic black mass calculated based on the mixing ratio. This composition indicates that blended chemical powders simulate typical NMC 811-type cathode materials. The high carbon content (28.3 wt %) simulates anode materials (graphite and conductive carbon), and the fluorine content (1.34 wt %) originates from the PVDF binder, replicating industrial residues.

Table 1. Calculated Elemental Composition of Synthetic Black Mass

Li (wt %)	Co (wt %)	Ni (wt %)	Mn (wt %)	C (wt %)	F (wt %)	H (wt %)	O (wt %)
5.04	4.24	33.8	3.95	28.3	1.34	0.03	23.0

Table 2 presents the results of the chemical composition for the industrial BM. The analysis indicates that the BM contains a high concentration of Ni, alongside Co, Li, and Mn. The presence of carbon at 32.3 wt % confirms the presence of graphite anode material. Additionally, Al is present at 0.56 wt % from the cathode foil, while Cu from the anode foil is present at 0.32 wt %. Low levels of Ca are also present at 0.35 wt %. The presence of Ca and Al is significant as these elements form stable fluoride compounds such as calcium fluoride, CaF_2, and AlF_3 that immobilize fluorine in condensed phases,[12] acting as fluorine scavengers during thermal treatment. F is present at 0.63 wt %, primarily from $LiPF_6$ and associated fluorinated binders. The relatively low fluorine content reflects electrolyte and binder degradation during battery use and preprocessing of the material.

Table 2. Chemical Composition of Industrial Black Mass

Li (wt %)	Co (wt %)	Ni (wt %)	Mn (wt %)	Cu (wt %)	Ca (wt %)	Al (wt %)	F (wt %)	C (wt %)
4.69	5.90	38.2	3.36	0.32	0.35	0.56	0.63	32.3

The diffractogram in Figure 1 shows the diffraction peaks for Li[$Ni_xMn_yCo_z$]O_2 and graphite. These peaks indicate that the black mass contains the cathode material commonly found in nickel−manganese-cobalt (NMC) batteries and graphite, typically used as the anode material.

3.2. Thermodynamic Calculations. Figure 2 presents the results of thermodynamic calculations for $LiPF_6$ at every 25 °C in the range of 25−600 °C in 100 vol % N_2 and the mixture of 90 vol % N_2 and 10 vol % H_2. As shown in Figure 2a, PF_5(g) is the predominant gas-phase species. Its mass remains constant at 0.83 g across the temperature range, indicating that, under inert conditions, $LiPF_6$ decomposes primarily into gaseous PF_5 and solid LiF, with 83 wt % of the total mass in the gas phase.

The calculations for $LiPF_6$ in a mixture of 90 vol % N_2 and 10 vol % H_2 presented in Figure 2 (b) indicate that PF_3 (g) is the dominant gaseous species in the range of 225 to 600 °C, while HF(g) is estimated to be present in lower quantities. PF_5 (g) is found in the calculation results in the temperature range

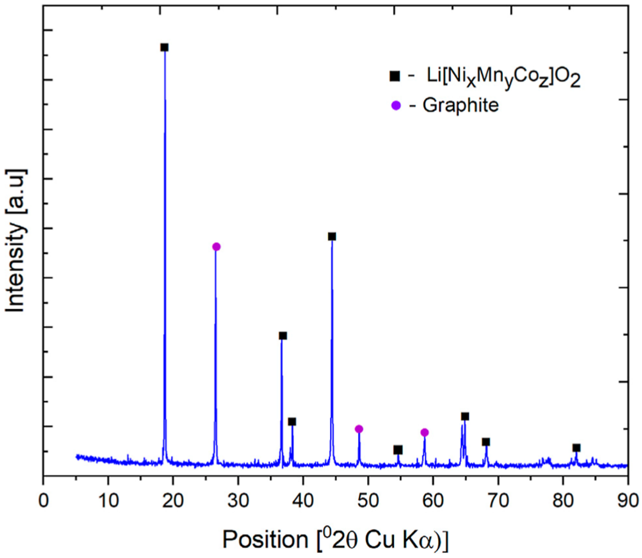

Figure 1. Diffractogram of industrial black mass from spent LiBs.

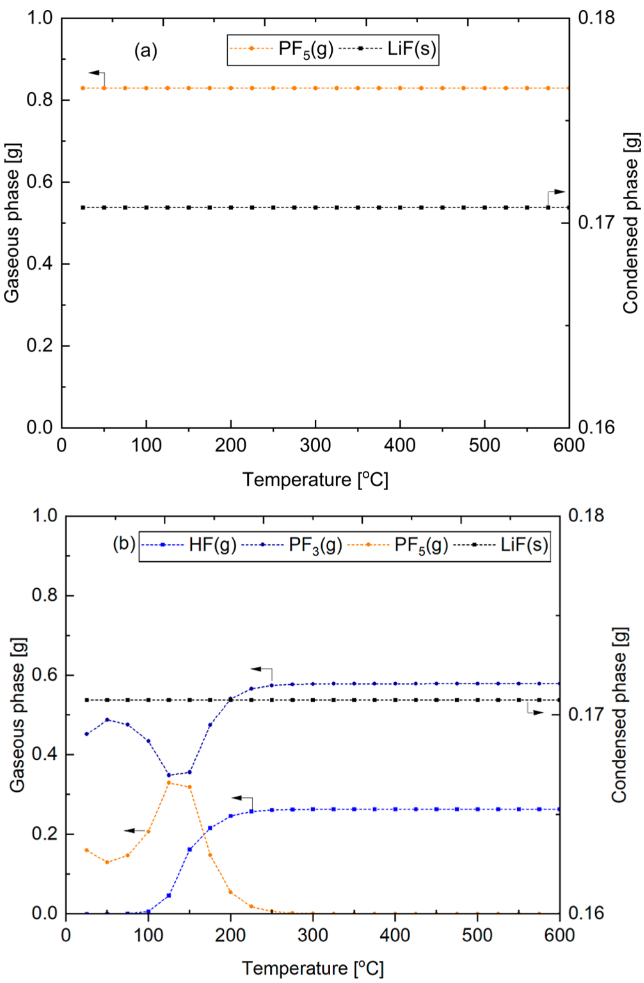

Figure 2. Calculated mass of the gaseous species for $LiPF_6$ at temperatures between 25 and 600 °C in (a) 100 vol % N_2, (b) 90 vol % N_2 −10 vol % H_2.

of 25 to 225 °C. The estimated amounts of H_2 (not presented in Figure 2) are low, e.g. 0.02 g at 150 °C and 0.03 g at 300 °C, which is calculated for all temperatures up to 600 °C. This indicates that 70 wt % of the introduced H_2 is present as free gas at temperatures above 300 °C, while the remaining 30 wt % is estimated to participate in reactions. These results indicate that for both calculation cases, $LiPF_6$ is not thermodynamically stable under the calculated conditions. Therefore, the calculations suggest that PF_5 and LiF will form when kinetically feasible, and in the case of the presence of H_2, PF_5 can react, forming PF_3 and HF.

Figure 3 presents the estimated amount of the gaseous species for PVDF heated up to 600 °C in (a) 100 vol % N_2 and

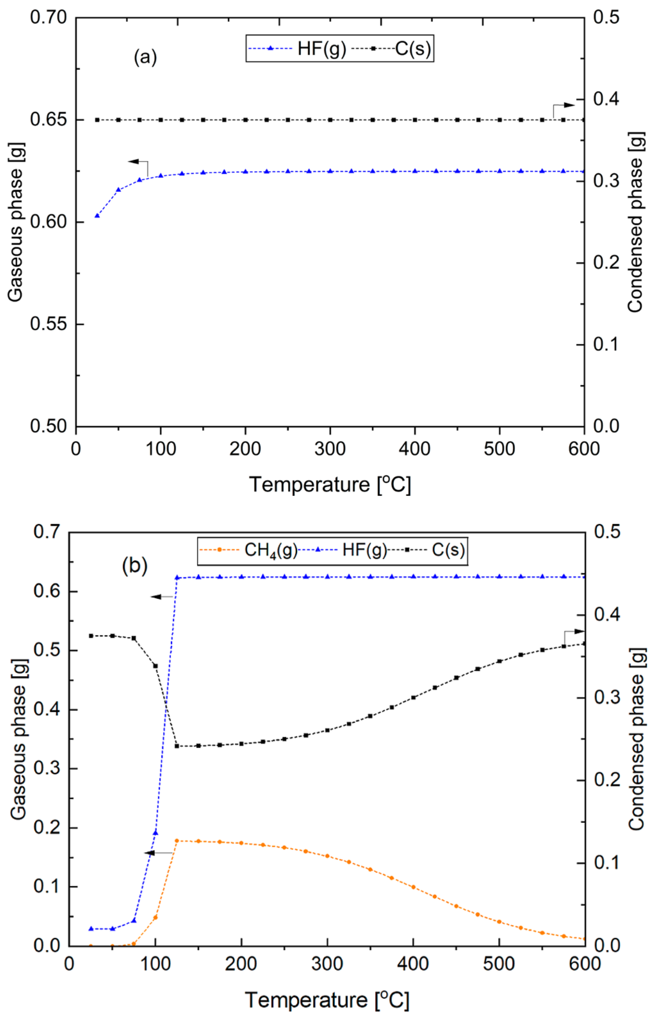

Figure 3. Calculated mass of gaseous species for PVDF heated up to 600 °C under (a) 100 vol % N_2, (b) 90 vol % N_2-10 vol % H_2.

(b) a mixture of 90 vol % N_2 −10 vol % H_2. Figure 3a indicates that HF(g) is the dominant gaseous species, with its mass 0.60 g at 25 °C, and remains constant at 0.63 g above 150 °C. Carbon remains constant at 0.37 g across the entire temperature range. This indicates that 63 wt % of the total calculated species mass at 600 °C is in the gas phase. Figure 3b presents the calculated gaseous PVDF species in 90 vol % N_2 −10 vol % H_2. The calculation indicates that HF is the primary species generated from PVDF, and it remains constant at temperatures ranging from 125 to 600 °C at 0.63 g. The estimated amount of H_2 in the gas phase is low at lower temperatures; at 500 and 600 °C, it is estimated to be 0.03 and 0.04 g, respectively. The condensed fraction consists of solid carbon, which is 0.24 g at 150 °C, 0.30 g at 400 °C, and 0.37 g at 600 °C. Approximately 63 wt % of the total calculated species mass is in the gas phase at 600 °C.

The thermodynamic calculations for the synthetic black mass, every 25 °C between 25 and 600 °C in 100 vol % N_2 and a mixture of 90 vol % N_2 and 10 vol % are presented in Figure 4. Figure 4 (a) shows that calculations estimate a minimal gas phase at 25 °C in an inert atmosphere. Besides the N_2, CO_2 dominates in the gaseous phase at high temperatures, with the highest value of 0.06 g calculated for the equilibrium at temperatures between 250 and 350 °C. Above 500 °C, CO dominates, e.g 0.08 g at 600 °C, while CO_2 is 0.02 g, other species (H_2, CH_4, HF) are present at amounts below 0.001 g. The condensed phase estimated to consist of C(s), Li_2CO_3(s), LiF(s), $MnCO_3$(s), CoO(s), Ni(s), and NiO(s), is higher at lower temperatures, with 0.85 g at 200 °C, while reaching 0.77 g at 600 °C. Figure 4b indicates that when the synthetic black mass is heated to 600 °C in 90 vol % N_2-10 vol % H_2 atmospheres, besides N_2, HF(g) and CH_4(g) predominate in the gas phase. At lower temperatures, CH_4(g) dominates with 0.17 g present at 25 °C. At higher temperatures, the amount is lower, with 0.04 g at 500 °C and 0.01 g at 600 °C. Above 300 °C, CO becomes the dominant gaseous component, exceeding the amount of CH_4 at 500 °C, where it reaches 0.06 g at 600 °C. The estimated amount of H_2 in the gas phase is relatively low at 25 °C, indicating that most of the H_2 is part of CH_4, which is more prevalent at lower temperatures, with 0.24 g at 200 °C. At higher temperatures, H_2 in the gas phase is estimated to be higher, with 0.02 g at 400 °C and 0.06 g at 600 °C, indicating that nearly 90 wt % of the introduced H_2 is present in the gas phase. In contrast, CO_2 levels are comparatively lower, with a maximum of 0.01 g at 600 °C. HF remains present in small quantities throughout the temperature range. The amount of condensed phase is estimated to be higher at low temperatures, with 0.84 g at 100 °C and reaching low levels of 0.78 g at 600 °C.

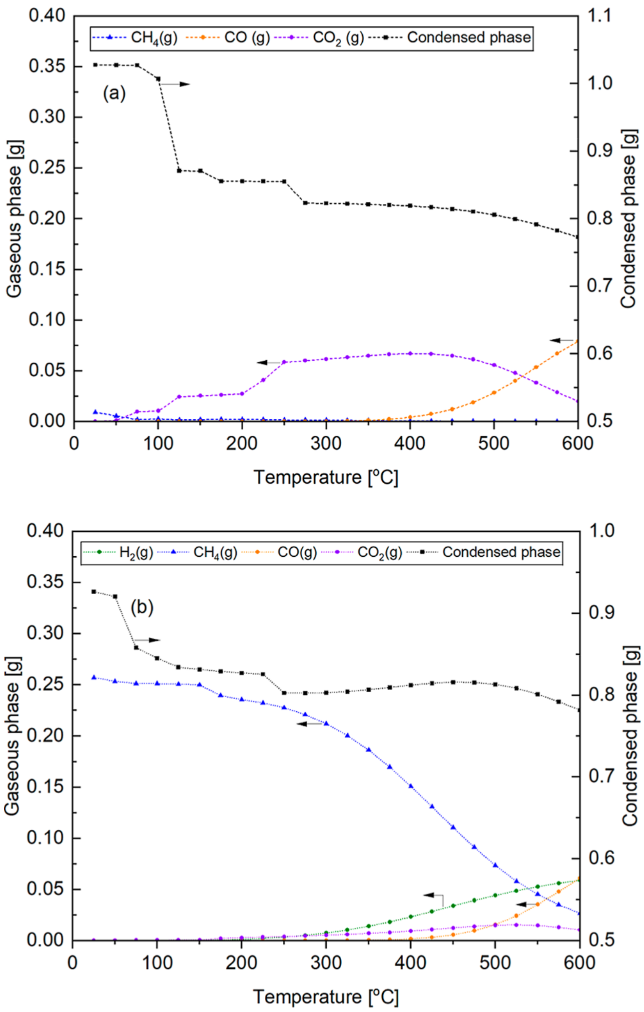

Figure 4. Calculated mass of gaseous and condensed phase for synthetic black mass in (a) 100 vol % - N_2, (b)90 vol % N_2-10 vol % H_2.

Thermodynamic calculations for LiBs black mass at each temperature between 25 and 600 °C, assuming in (a)100 vol % N_2 and (b) 90 vol % N_2-10 vol % H_2, are presented in Figure 5.

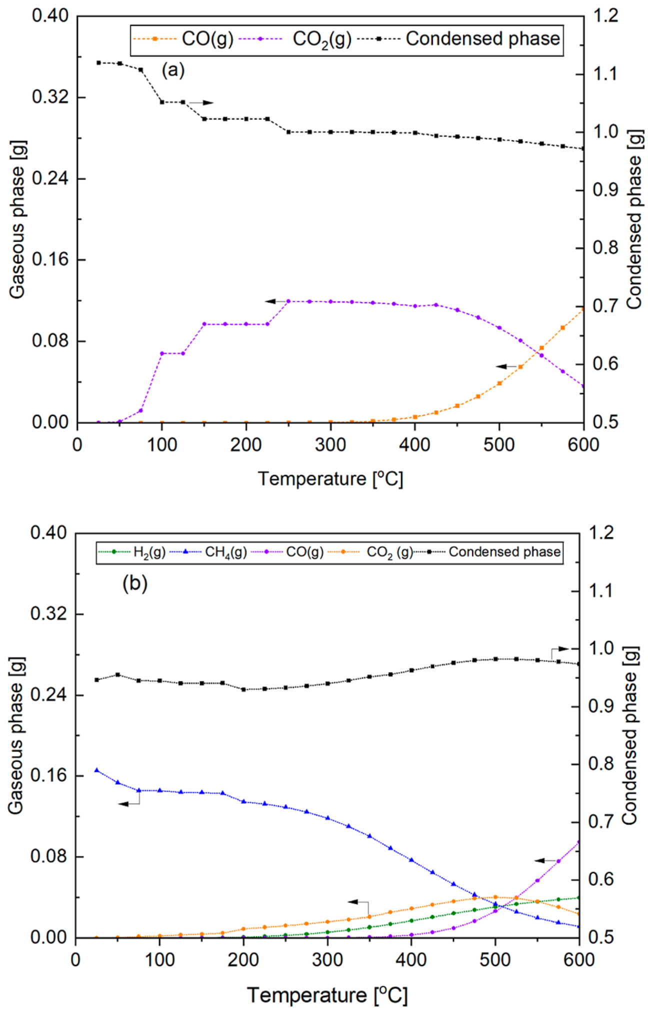

Figure 5. Calculated mass of black mass heated up to 600 °C under (a) 100 vol % N_2 (b) 90 vol % N_2 −10 vol % H_2.

The calculations indicate that the black mass is almost entirely solid throughout the temperature range of 25 to 600 °C, with the condensed fraction consistently being around 0.93 g. The gas phase estimate is, besides N_2, mainly composed of CO_2 and CO, with 0.04 g estimated at 100 °C, 0.06 g at 250 °C, and only 0.01 g at 600 °C. CO(g) is estimated to be 0.06 g at 400 °C and reaches 0.06 g at 600 °C. When assuming an atmosphere containing 90 vol % N_2 and 10 vol % H_2, as presented in Figure 5b, the calculations show that CH_4 is the

https://doi.org/10.1021/acssuschemeng.5c10344
ACS Sustainable Chem. Eng. XXXX, XXX, XXX−XXX

dominant generated gaseous compound at lower temperatures, with 0.17 g at 25 °C. This concentration is lower at higher temperatures, reaching 0.08 g at 400 °C and 0.01 g at 600 °C. Additionally, trace amounts of H_2O and CO are estimated to be present in the gaseous phase at temperatures above 300 °C. The condensed phase estimated to be composed of C(s), Li_2CO_3(s), LiF(s), CaF_2(s), MnO(s), $LiAlO_2$(s) Ni(s), Cu(s), Co(s) and CoO (s). The calculations indicate that its mass is higher at high temperatures, from 0.93 g at 200 °C to 0.96 g at 400 °C and 0.97 g at 600 °C. This increase at higher temperatures, particularly beyond 400 °C, is primarily attributed to the deposition of solid carbon. At lower temperatures, CH_4 (g) is the dominant generated gas-phase specie, however, as the temperature rises, its calculated mass decreases while the mass of solid carbon increases. This trend reflects the thermodynamically favored decomposition of CH_4 into solid carbon and hydrogen gas, which contributes to the higher mass for the condensed phase.

3.3. Thermogravimetric and Mass Spectrometry Analysis for Evolved Gases. The thermogravimetric analysis (TGA) of $LiPF_6$, conducted in both 100 vol % N_2 and a 90 vol % N_2 and 10 vol % H_2 atmosphere as presented in Figure 6,

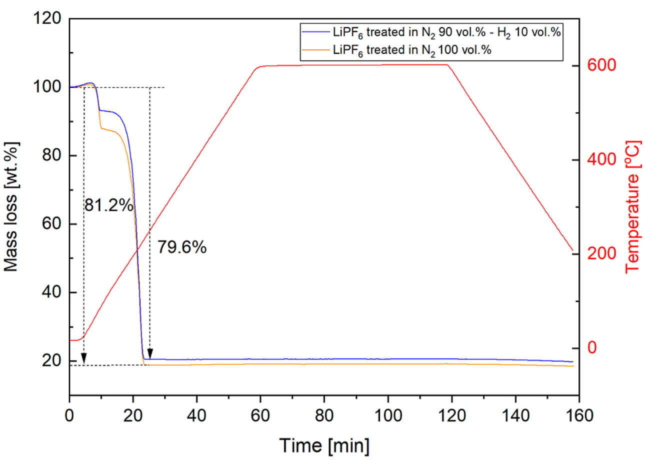

Figure 6. TGA curve for $LiPF_6$ heated under 100 vol % N_2 and in 90 vol % N_2 −10 vol % H_2.

indicates a different two-step mass loss behavior, with differences in the initial behavior influenced by the gas composition. The apparent increase in mass that occurs between 5 and 10 min is due to a buoyancy effect commonly observed in TGA, caused by changes in gas density as the furnace heats. In both atmospheres, the initial mass loss begins at approximately 86.9 °C, corresponding to the release of volatile fluorine-containing components. However, the extent of the first mass loss varies, with 11.3 wt % being lost in the 100 vol % N_2 atmosphere, while only 6.77 wt % is lost in the N_2 and H_2 mixture. The second mass loss step occurs between 87 and 232 °C and is attributed to the thermal decomposition of $LiPF_6$ into volatile fluorinated species, such as PF_5, leaving behind a thermally stable LiF residue. The total mass loss is essentially the same under both atmospheres, with 81.2 wt % in 100 vol % and 79.5 wt % in a mixture of 90 vol % N_2 and 10 vol % H_2. The small difference is likely attributed to initial variation caused by buoyancy effects in the TGA.

Figure 7 presents the QMS data for the gaseous species detected when $LiPF_6$ is heated to 600 °C in two different atmospheres. The monitored QMS data presented in Figure 7

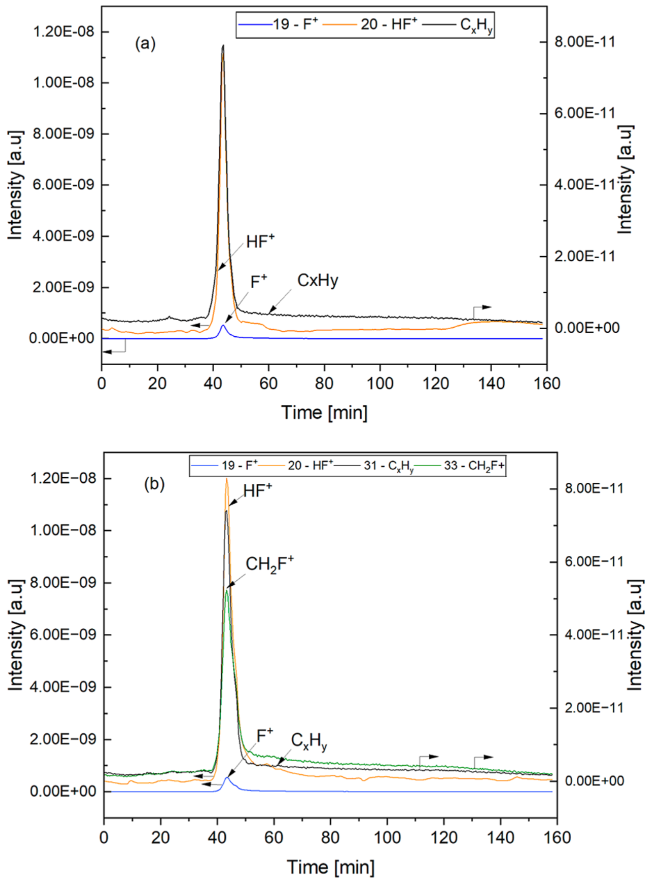

Figure 7. QMS for $LiPF_6$ heated under (a) 100 vol % N_2 (b) 90 vol % N_2-10 vol % H_2.

(a) for $LiPF_6$ heated in a 100 vol % N_2 atmosphere, corresponding to the TGA curve in Figure 6, indicate peaks at m/z = 19 (F^+), m/z = 50 (PF_5^+), which correspond to fluoride ions (F^+) and phosphorus pentafluoride (PF_5), respectively. These peaks confirm the primary decomposition of $LiPF_6$ into PF_5 and LiF, with PF_5 volatilising and fragmenting into F-containing species. The QMS data presented in Figure 7 (b) for $LiPF_6$ heated in the atmosphere containing a mixture of 90 vol % N_2 and 10 vol % H_2, as shown in the TGA curve in Figure 6, indicates peaks m/z = 19 (F^+) and m/z = 50 (PF_5^+) with an additional peak at m/z = 20 (HF^+), which corresponds to hydrogen fluoride. Additionally, the PF_5^+ signal in the H_2-containing atmosphere is broader and more sustained, suggesting that the presence of hydrogen may alter secondary decomposition reactions. However, the nearly identical and overlapping TGA mass loss curves in both atmospheres indicate that the fundamental decomposition mechanism of $LiPF_6$ is similar, and that hydrogen primarily influences gas-phase reactions with the evolved species rather than the decomposition steps of $LiPF_6$.

Figure 8 presents the TGA profiles of PVDF samples heated to 600 °C under two different atmospheres, but with nearly identical mass loss of 63.5 wt % in 100 vol % N_2 and 63.7 wt % in the N_2 and H_2 mixture. The degradation begins at a similar temperature for both atmospheres, indicating that the presence of hydrogen does not influence the thermal stability of PVDF. The mass loss behavior can be divided into two distinct regions. The first region, between about 400 and 500 °C, is marked by rapid and substantial mass loss, which correlates

https://doi.org/10.1021/acssuschemeng.5c10344
ACS Sustainable Chem. Eng. XXXX, XXX, XXX−XXX

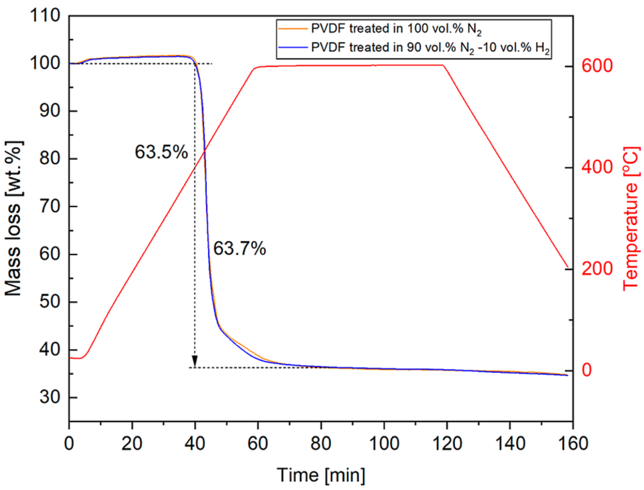

Figure 8. TGA curve for PVDF heated under 100 vol % N_2 and in a mixture of 90 vol % N_2 −10 vol % H_2.

with the primary decomposition of PVDF involving the release of volatile compounds, including HF. The second region, from 500 to 620 °C, extends through the isothermal hold and exhibits a significantly slower and more gradual mass loss. This phase indicates the breakdown of more thermally stable PVDF residues. The gradual mass increase observed between 5 and 40 min is attributed to a buoyancy effect in the TGA. As the gas density decreases with increasing temperature, the sample experiences a transient apparent mass gain, which is an instrument effect and not a real mass increase.

Figure 9 presents QMS data for PVDF heated under 100 vol % N_2 and 90 vol % N_2, and 10 vol % H_2 atmospheres. In both environments, a major gas evolution event occurs between 400 and 500 °C, where the principal mass loss region is observed in the TGA in Figure 8. The monitored QMS data presented in Figure 9a for PVDF heated in a 100 vol % N_2 atmosphere show peaks at m/z = 19 (F^+), m/z = 20 (HF^+), and m/z = 31 (C_xH_y). These peaks correspond to fluoride ions, hydrogen fluoride (HF), and hydrocarbon (C_xH_y) fragments, respectively. The presence of these peaks indicates that the decomposition of PVDF leads to the release of fluorine-containing compounds, with HF being a primary gaseous product. In Figure 9b, the QMS data for PVDF heated in a 90 vol % N_2 and 10 vol % H_2 atmosphere reveal similar peaks at m/z = 19 (F^+), m/z = 20 (HF^+), and m/z = 31 (CxHy), along with an additional peak at m/z = 33 (CH_2F^+), which corresponds to fluoroalkyl species. The presence of this additional peak in the hydrogen-containing environment suggests that hydrogen may react with the released gases during the decomposition of PVDF. However, the primary decomposition pathway of PVDF remains the same in both atmospheres.

Figure 10 presents the TGA profiles of the synthetic black mass composed of 70 wt % $LiNiCoMnO_2$, 5.0 wt % activated carbon, 25 wt % graphite, 1.0 wt % $(C_2H_2F_2)$n, and 1.0 wt % $LiPF_6$, heated to 600 °C under two different atmospheres. When heated in 100 vol % N_2, the material experiences a total mass loss of 2.68 wt %. This process occurs in distinct stages, with the first stage taking place between 25 and 150 °C, resulting in a mass loss of 1.0 wt %, likely due to the evaporation of residual electrolyte solvents. A slight apparent increase in mass is also observed between 5 and 10 min due to the buoyancy effect. Between 150 and 400 °C, the mass

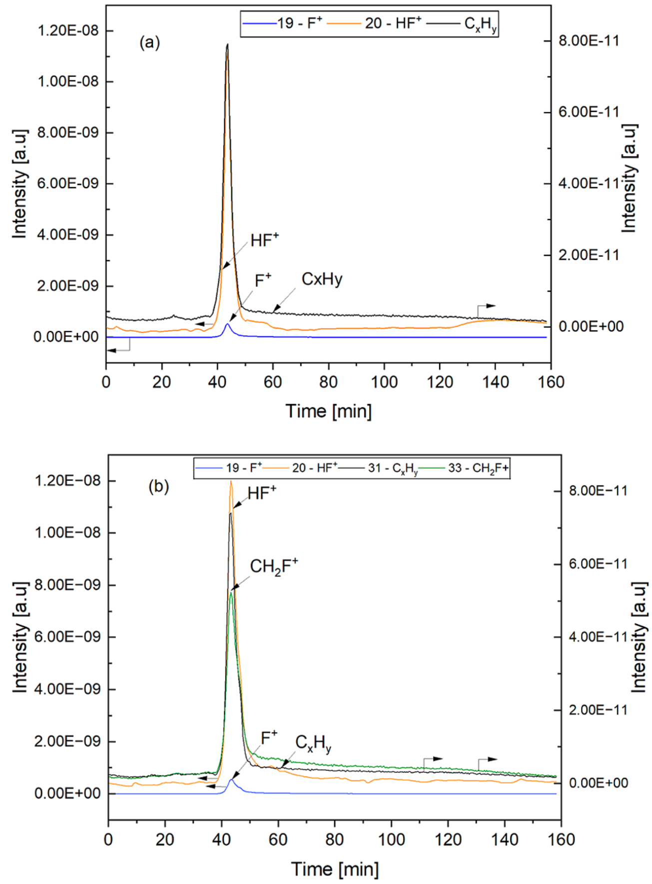

Figure 9. QMS data for PVDF heated under (a) 100% N_2 (b) 90% N_2-10% H_2.

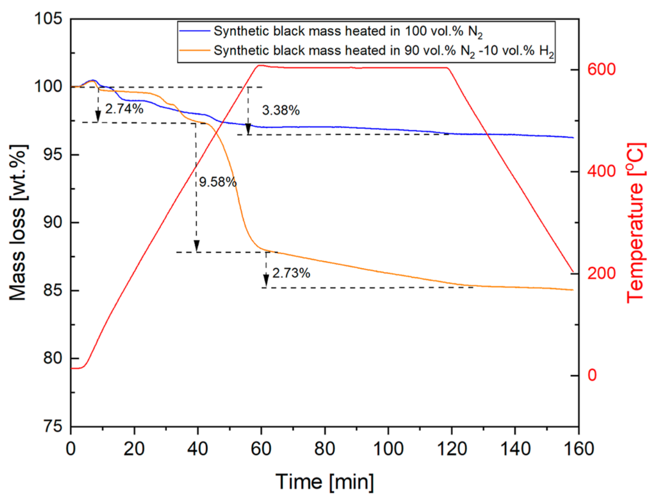

Figure 10. TGA profile for synthetic black mass heated under 100 vol % N_2 and in a mixture of 90 vol % N_2 −10 vol % H_2.

remains stable, as graphite, activated carbon, and the cathode material are inert within this temperature range. Between 400 and 510 °C, 1.5 wt % is lost, likely due to the degradation of PVDF. In the final stage, from 510 to 600 °C, the sample remains stable, with a negligible mass loss of 0.20 wt %. In a mixture of 90 vol % N_2 and 10 vol % H_2, a mass loss of 1.0 to 1.2 wt % occurs up to approximately 150 °C, primarily due to the decomposition of $LiPF_6$. Between 150 and 350 °C, a further mass loss occurs, reaching a total of about 2.5 wt %, which can primarily be attributed to the decomposition of the PVDF. In the temperature range of 400 to 500 °C, a significant mass loss of around 6 wt % occurs, mainly due to the decomposition of the PVDF binder and the hydrogen-assisted reduction of the $LiNiCoMnO_2$ cathode material. During the final holding period between 500 and 600 °C, an additional 2.4 wt % is lost as the reduction reactions of transition-metal oxides continue, and the remaining PVDF completes its decomposition. These findings indicate that the presence of hydrogen alters the thermal behavior of synthetic black mass, leading to sequential mass loss stages that mainly reflect the reduction of metal oxides.

Figure 11 presents the QMS data for the synthetic black mass, which shows a strong initial signal for m/z = 44, which corresponds to CO_2. This early release of CO_2 is likely attributed to the release of gases that were adsorbed onto the surface of activated carbon.[28] Additional minor CO_2 signals appear periodically throughout the heating process, indicating a gradual decomposition reaction. However, the main components of the synthetic black mass, such as graphite and $LiNiCoMnO_2$, remain chemically inert in N_2 atmosphere for temperatures below 600 °C. In a 90 vol % N_2 and 10 vol % H_2 atmosphere, the QMS shows signals for CH_4 (m/z = 16), H_2O (m/z = 18), and CO_2 (m/z = 44). The CO_2 signal appears early, similar to that in an N_2 atmosphere. An H_2O peak emerges corresponding to the temperature range of 400–500 °C, likely correlating with the reductive decomposition of $LiNi_xCo_yMn_zO_2$.

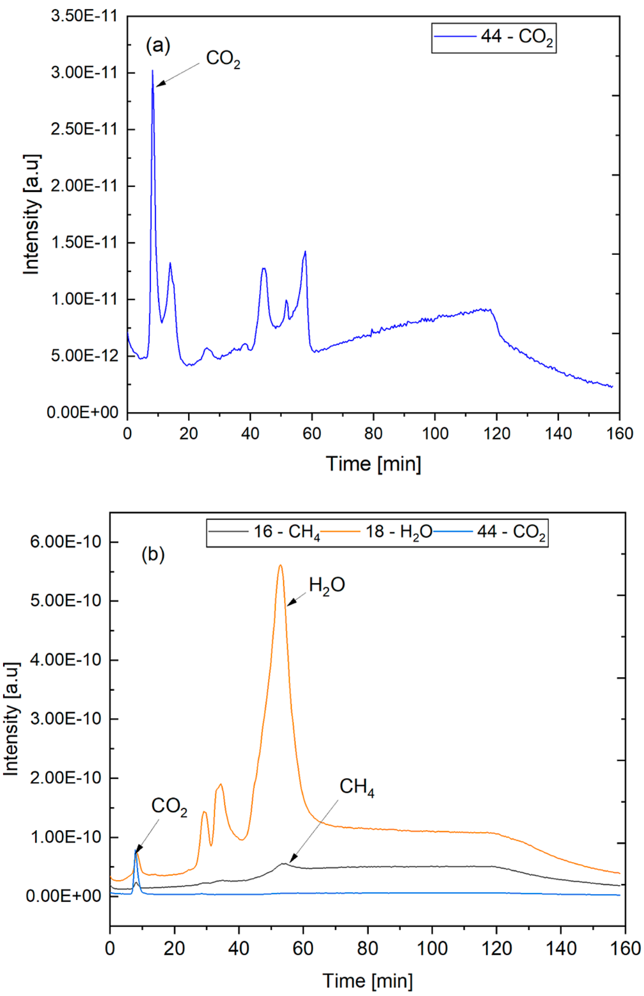

Figure 11. QMS data for Synthetic black mass heated under (a) 100 vol % N_2 (b) 90 vol % N_2-10 vol % H_2.

Figure 12 presents the TGA results for black mass heated in 100 vol % N_2 and a mixture of 90 vol % N_2 with 10 vol % H_2.

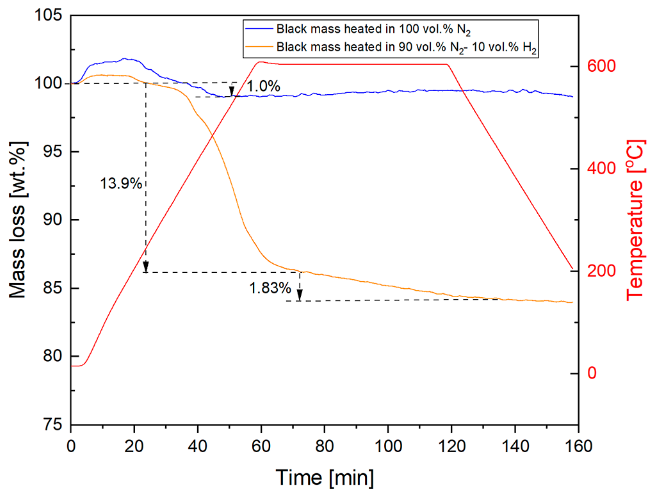

Figure 12. TGA profile for black mass heated under 100% N_2 and in a mixture of 90% N_2 −10% H_2.

In both atmospheres, the temporary rise in mass is observed during the initial stages of heating due to buoyancy effects. Under N_2, the industrial black mass shows a total mass loss of approximately 1.0 wt %, which is attributed to the removal of moisture and residual electrolyte solvents and is considerably lower than the 3.38 wt % recorded for the synthetic black mass. This difference can be explained by variations in fluorine and binder composition. The synthetic black mass contains a higher proportion of $LiPF_6$ and PVDF of 1 wt % each, corresponding to about twice the total fluorine content of the industrial sample (1.34 wt % vs 0.63 wt %). The industrial black mass also contains 0.35 wt % Ca and 0.56 wt % Al, both of which can stabilize fluorine within condensed fluoride phases such as CaF_2, AlF_3, and LiF under inert conditions. When considered relative to their fluorine content, both materials would exhibit similar decomposition trends, indicating that the larger mass loss of the synthetic black mass primarily arises from its greater fluorine content and lack of fluoride-stabilizing phases. Between 380 and 600 °C, the sample in the H_2-containing atmosphere experiences a significant weight loss of 12.7 wt %. This loss is attributed to the reduction of metal oxides, mainly Ni^{3+} to Ni^{2+}/Ni with small contributions from cobalt oxide reduction, CoO/Co, and the decomposition of PVDF. During the isothermal hold at 600 °C, black mass samples treated in the H_2-containing atmosphere undergo an additional weight loss of 1.85 wt % due to the continued and slow reduction of metal oxides.

Figure 13 presents QMS data for industrial black mass heated under 100 vol % N_2 and in a mixture of 90 vol % N_2 and 10 vol % H_2 corresponding to the TGA in Figure 12. In 100 vol % N_2, the QMS in Figure 13 (a) indicates the detection of carbon dioxide (CO_2, m/z = 44) with peaks observed between 200 and 400 °C, indicating the release of CO_2, possibly originating from organic solvents in the electrolyte, such as ethylene carbonate and dimethyl carbonate, which can thermally decompose at these temperatures.[29] In the H_2-containing atmosphere presented in Figure 13 (b), strong

https://doi.org/10.1021/acssuschemeng.5c10344
ACS Sustainable Chem. Eng. XXXX, XXX, XXX−XXX

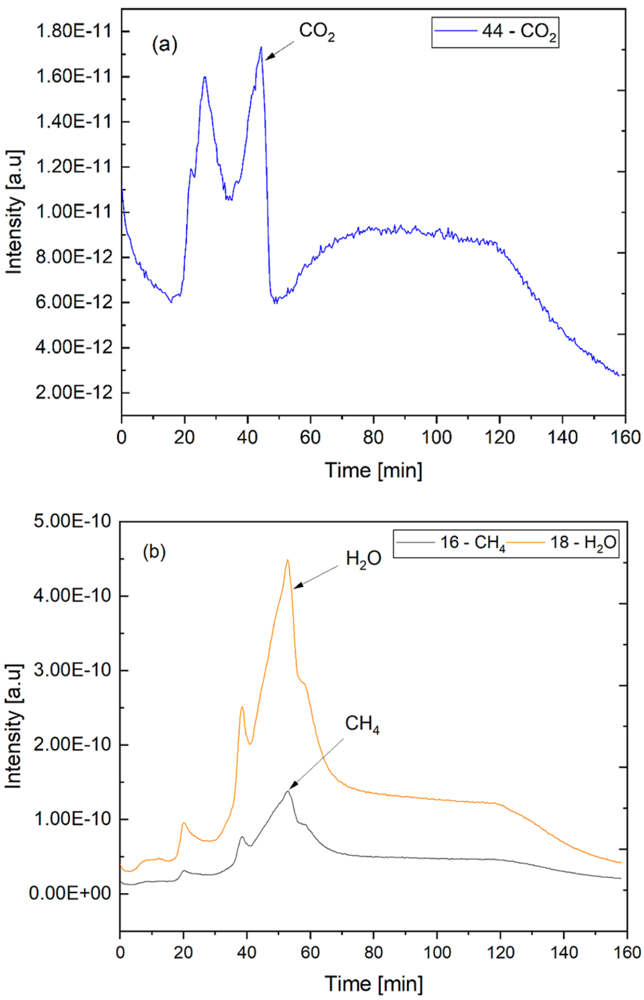

Figure 13. QMS data for Black mass heated under (a) 100 vol % N_2 (b) 90 vol % N_2-10 vol % H_2.

peaks for water (H_2O, m/z = 18) and methane (CH_4, m/z = 16) are observed, indicating that hydrogen reacts with oxygen liberated from metal oxides to form H_2O, which subsequently participates in secondary reactions with residual carbon to produce CH_4.

Table 3 summarizes the thermal behavior of LiBs materials heated to 600 °C in 2 atm. In pure N_2, carbon-based materials show minimal decomposition, while fluorinated compounds like $LiPF_6$ and PVDF experience significant mass loss and release of hydrogen fluoride (HF). In an H_2-containing atmosphere, both $LiPF_6$ and PVDF exhibit similar mass loss to that observed in N_2, while synthetic and industrial black mass samples show significantly higher weight loss. The increased mass loss is primarily due to the reduction of metal oxides, mainly nickel oxides and cobalt oxides, as well as from the thermal decomposition of residual organic materials. These reactions generate significant amounts of gaseous CO_2, H_2O, and CH_4, contributing directly to the measured weight loss.

4. DISCUSSION

The TGA results indicate that heating black mass in a 100% N_2 atmosphere leads to minimal weight loss and the release of CO_2, as revealed by the TGA in Figure 12 and the QMS data shown in Figure 13a respectively.

Figure 13This black mass is predominantly composed of metal oxides from $Li[Ni_xMn_yCo_z]O_2$ cathode materials. Among these, Ni is the most abundant at 38.2 wt %, followed by Co at 5.90 wt % and Mn at 3.36 wt %. These metal oxides contain significant amounts of lattice oxygen, which becomes available for release upon heating.[30,31] Theoretical calculations estimate that the industrial black used in this study contains 26.0 wt % of oxygen bound to these metal oxides. Upon heating, this oxygen can combine with the residual carbon content of 32.3 wt % to generate CO_2. However, the experimentally observed weight loss is significantly lower than expected for such a redox process. This difference suggests that the CO_2 detected in QMS is not primarily a result of lattice oxygen reacting with carbon but originates from the

Table 3. Thermal Behaviour of LiBs Components Heated up to 600 °C in Inert and H_2-Containing Atmosphere

material	composition	treatment conditions	weight loss (wt %)	ionised off-gases (m/z)
graphite	C − 99.9 wt %	100 vol %N_2	0.13	-
activated carbon	C − 99.9 wt %	100 vol % N_2	2.95	-
electrolyte ($LiPF_6$)	Li − 4.57 wt %, P − 20.4 wt %, F − 75.1 wt %	100 vol % N_2	79.6	19 (F^+), 50 (PF^+)
electrolyte ($LiPF_6$)	Li − 4.57 wt %, P − 20.4 wt %, F − 75.1 wt %	90 vol % N_2/10 vol % H_2	81.2	19 (F^+), 20 (HF^+), 50 (PF^+)
PVDF $(C_2H_2F_2)_n$	C − 37.5 wt %, H − 3.10 wt %, F − 37.9 wt %	100 vol % N_2	63.5	18 (H_2O^+), 19 (F^+), 20 (HF^+)
PVDF $(C_2H_2F_2)_n$	C − 37.5 wt %, H − 3.10 wt %, F − 37.9 wt %	90 vol % N_2/10 vol % H_2	63.7	18 (H_2O), 19 (F^+), 20 (HF^+), 31(C_xH_y)
synthetic black mass	Li − 5.04 wt %, Ni − 33.8 wt %, Co − 4.24 wt %, Mn − 3.95 wt %, C − 28.3 wt %, F − 1.34 wt %, H − 0.03 wt %, O − 23.0 wt %	100 vol % N_2	3.38	44 (CO_2)
synthetic black mass	Li − 5.04 wt %, Ni − 33.8 wt %, Co − 4.24 wt %, Mn − 3.95 wt %, C − 28.3 wt %, F − 1.34 wt %, H − 0.03 wt %, O − 23.0 wt %	90 vol % N_2/10 vol % H_2	15.1	16 (CH_4^+), 18 (H_2O^+), 44 (CO_2)
black mass	Li − 4.69 wt %, Ni − 38.2 wt %, Co − 5.90 wt %, Mn − 3.36 wt %, C − 32.3 wt %, F − 0.63 wt %.	100 vol % N_2	1.00	44 (CO_2)
black mass	Li − 4.69 wt %, Ni − 38.2 wt %, Co − 5.90 wt %, Mn − 3.36 wt %, C − 32.3 wt %, F − 0.63 wt %.	90 vol % N_2/10 vol % H_2	15.7	16 (CH_4^+), 18 (H_2O^+)

https://doi.org/10.1021/acssuschemeng.5c10344
ACS Sustainable Chem. Eng. XXXX, XXX, XXX−XXX

thermal decomposition of organic electrolyte residues, such as ethylene carbonate and dimethyl carbonate, which volatilize and decompose within the 200−400 °C temperature range. This also reflects a deviation between the thermodynamic predictions and the experimental findings. Thermodynamic models predict 0.96 g of solids remaining at 400 °C, corresponding to approximately 4 wt % gas release, whereas experimental results indicate about 15 wt % total mass loss. This difference is attributed to the simplified assumptions in the equilibrium calculations and to the volatile components in the industrial black mass, which were not accounted for in thermodynamic calculations.

Studies have also indicated that when black mass is heated in an inert atmosphere below 400 °C, it undergoes minimal mass loss, largely because its main component, the cathode material, remains structurally stable under these conditions.[32,33] According to the study,[34] structural changes in cathode material begin to occur when heated in an inert atmosphere beyond 600 °C, with TG-DSC analysis revealing minor mass loss events accompanied by exothermic peaks, indicating the onset of thermal transitions. Parallel XRD analysis shows phase transitions from the original layered structure to more disordered phases such as spinel. These observations support the TGA results and the earlier findings,[32,33] which reported minimal mass loss below 400 °C, primarily due to the structural stability of the cathode materials under inert conditions. While NMC-type cathodes remain largely stable and retain their layered or partially disordered structure below 400 °C, further heating above 600 °C drives the transition to simple oxide phases such as NiO and CoO, particularly in the presence of reducing agents like Carbon. Thermodynamically, the reduction of NiO and CoO in NMC black mass by solid carbon becomes favorable above 600 °C, particularly reduction occurring between 800 and 1000 °C and requires the prior decomposition of NMC into its corresponding simple oxides.[35] However, the direct reduction of intact or partially disordered NMC by solid carbon faces significant kinetic barriers, primarily due to restricted surface contact and interaction between solid carbon and cathode particles, and strong metal−oxygen bonds that require high activation energy to break. The presence of H_2, even at low partial pressures such as 10 vol %, fundamentally changes the reduction mechanism and kinetics. Reduction of NiO and CoO by H_2 is thermodynamically favorable at much lower temperatures, between 400−500 °C.[36,37] Under this temperature range, H_2 readily diffuses to oxide surfaces and reacts, overcoming kinetic barriers that limit solid−solid reactions.[38] This is why the QMS results in

Figure 13b show H_2O evolution and significant mass loss during heating in H_2/N_2 mixtures at 400−600 °C, confirming the reduction of Ni and Co oxides by H_2 as described in eqs 1 and 2.

$$NiO(s) + H_2(g) \rightarrow Ni(s) + H_2O(g) \tag{1}$$

$$CoO(s) + H_2(g) \rightarrow Co(s) + H_2O(g) \tag{2}$$

Stoichiometric calculation based on the industrial black mass composition (Table 2) also supports these reduction mechanisms. For a 100 g black mass sample containing 38.2 wt % Ni, 5.9 wt % Co, and 3.36 wt % Mn, complete reduction of NiO and CoO would remove about 12.0 g of oxygen. This theoretical range closely matches the observed 12.7 wt % mass loss in H_2 (Figure 12), confirming that oxygen removal through the reduction of Ni, Co oxides is the main cause of mass loss under reducing conditions.

The QMS results in Figure 13b show that gas evolution begins with the release of H_2O, followed by CH_4. This sequence indicates that methane formation is a secondary process, and not a primary decomposition product, and arises from reactions involving residual carbon and H_2O. Particularly, H_2O generated through the reduction of metal oxides by hydrogen can react with carbon to produce CO. The resulting CO can then form CH_4 in the presence of H_2. Both reactions are thermodynamically favorable in the 300−600 °C range and are further promoted by the catalytic activity of transition metals such as Ni,[39] which are present in the industrial black mass. Experimental studies have also indicated that at temperatures above 700 °C, CH_4 becomes an active reductant for $Li(Ni_xCo_yMn_{1-y-x})O_2$ (NMC) as it transitions from a secondary product to an active reductant capable of directly engaging in reduction reactions.[40,41] Therefore, the QMS data revealing the presence of CH_4 in off-gases at temperatures below 600 °C indicate that CH_4 originates from secondary decomposition reactions involving water vapor produced in the first reactions. The relatively low concentrations of CH_4 and HF predicted in the thermodynamic simulations in Figures 4 and 5, compared to those observed in the experimental QMS in Figures 9 and 13, can be attributed to the limitations of the equilibrium approach. The model assumes complete thermodynamic equilibrium, neglecting the kinetic effects and decomposition pathways that dominate during actual heating. However, during experiments, these gases would be released even before the system reaches equilibrium. As a result, the experimental data captures these kinetically from the volatile products, whereas the model reflects the stable equilibrium composition achieved after the reactions have completed. The presence of Ca and Al in the black mass also affects its thermal behavior, particularly by forming stable fluoride phases such as CaF_2, and AlF_3 under inert conditions. These elements retain fluorine in the condensed phase, which minimizes volatile fluoride emissions. Thermodynamic calculations for the industrial black mass, as shown in Figure 5, indicate that these fluorides remain stable in an N_2 atmosphere. However, under an H_2-containing atmosphere, these compounds lose stability, leading to increased HF volatilisation. Previous studies indicate that adding calcium-based additives, such as calcium hydroxide ($Ca(OH)_2$), to black mass can effectively reduce HF emissions by immobilizing fluorine as CaF_2, achieving fixation efficiencies exceeding 98%.[42] In the absence of these additives, pyrolysis at temperatures between 300 and 600 °C can result in the loss of nearly 90 wt % of fluorine as HF and related gases, even in inert atmospheres.[43] This phenomenon explains why experimental results from a QMS in Figure 13a for industrial black mass heated in 100 vol % N_2 indicates that CO_2 is the predominant gas-phase species released primarily between 200 and 400 °C, with no detectable HF. This implies that fluorine remains bound in stable fluoride phases, confirming the stabilizing influence of Ca and Al when present in industrial black mass.

5. CONCLUSION

The present paper aimed to study the thermal behavior of LiBs black mass by analyzing the thermal behavior of its components when heated to 600 °C in both an inert (100 vol % N_2) atmosphere and a mixture of 90 vol % N_2 and 10 vol

https://doi.org/10.1021/acssuschemeng.5c10344
ACS Sustainable Chem. Eng. XXXX, XXX, XXX−XXX

% H_2. Based on the experiments and thermodynamic calculations, the following was concluded:

i. The breakdown of individual components offers valuable insights into the behavior of black mass. While graphite and activated carbon remain relatively stable in an inert atmosphere, $LiPF_6$ and PVDF experience significant mass loss due to the volatilisation of PF_5 and HF.
ii. In the presence of 10 vol % H_2, the reduction of Ni-metal oxides in both synthetic and industrial black mass becomes significant between 400 and 600 °C, leading to higher overall mass loss (15 wt %) and the evolution of H_2O and CH_4.
iii. Thermodynamic modeling of industrial BM confirmed that H_2 enhances Ni-oxide reduction and alters fluorine speciation by favoring PF_3 and HF formation, whereas under N_2 atmospheres fluorine is stabilized within condensed fluoride phases such as CaF_2, and AlF_3 in the presence of Ca and Al.
iv. These findings highlight that the thermal behavior of black mass is governed by its components and the presence of H_2 in the atmosphere, emphasizing the need to carefully balance the benefits of using reducing gases during the recycling process and the mitigation of releasing volatile fluorine.

ASSOCIATED CONTENT

Data Availability Statement

Supporting Information will be made available upon request.

AUTHOR INFORMATION

Corresponding Author

Moses Charles Siame − *Department of Civil, Environmental and Natural Resources Engineering, Minerals and Metallurgical Engineering, Process Metallurgy, Lulea University of Technology, Lulea 971 87, Sweden;* orcid.org/0009-0007-6714-944X; Email: moses.charles.siame@ltu.se

Authors

Hesham M. Ahmed − *Department of Civil, Environmental and Natural Resources Engineering, Minerals and Metallurgical Engineering, Process Metallurgy, Lulea University of Technology, Lulea 971 87, Sweden; Central Metallurgical Research and Development Institute, Helwan 11421, Egypt*

Anton Andersson − *Department of Civil, Environmental and Natural Resources Engineering, Minerals and Metallurgical Engineering, Process Metallurgy, Lulea University of Technology, Lulea 971 87, Sweden*

Lena Sundqvist-Öqvist − *Department of Civil, Environmental and Natural Resources Engineering, Minerals and Metallurgical Engineering, Process Metallurgy, Lulea University of Technology, Lulea 971 87, Sweden*

Complete contact information is available at: https://pubs.acs.org/10.1021/acssuschemeng.5c10344

Author Contributions

Moses C. Siame: Conceptualisation, methodology, formal analysis, investigation, data curation, writing of original draft preparation, review and editing, and visualization. **Hesham Ahmed**: Review, supervision, resources, project administration, and funding acquisition. **Anton Andersson**: Review, supervision, resources, and data curation. **Lena Sundqvist-Öqvist**: Review, supervision, resources, project administration, and funding acquisition.

Notes

The authors declare no competing financial interest.
The authors declare that they have no known competing financial interests or personal relationships that could have appeared to influence the work reported in this paper.

ACKNOWLEDGMENTS

This work was conducted within the Centre of Advanced Mining and Metallurgy (CAMM) at Luleå University of Technology. The authors would like to acknowledge the financial support provided by the Swedish Energy Agency under the project Optimising Processes for Recycling of lithium-ion batteries (OptiLIB). Additionally, the authors acknowledge the support from the Eco-friendly and Sustainable Method for Recycling Spent Lithium-Ion Batteries (EcoLIB) project, which is funded by the Interreg Aurora program (No. 20357954).

REFERENCES

(1) Lv, W.; Wang, Z.; Cao, H.; Sun, Y.; Zhang, Y.; Sun, Z. A Critical Review and Analysis on the Recycling of Spent Lithium-Ion Batteries. *ACS Sustainable Chem. Eng.* **2018**, *6* (2), 1504−1521.

(2) Roy, J.; Rarotra, S.; Krikstolaityte, V.; Zhuoran, K. W.; Cindy, Y. D.; Tan, X. Y.; Carboni, M.; Meyer, D.; Yan, Q.; Srinivasan, M. Green Recycling Methods to Treat Lithium-Ion Batteries E-Waste: A Circular Approach to Sustainability. *Adv. Mater.* **2021**, *34* (25), 2103346.

(3) Pinegar, H.; Smith, Y. End-of-Life Lithium-Ion Battery Component Mechanical Liberation and Separation. *JOM* **2019**, *71*, 4447−4456.

(4) Donnelly, L. J.; Pirrie, D.; Power, M.; Corfe, I.; Kuva, J.; Lukkari, S.; Lahaye, Y.; Liu, X.; Dehaine, Q.; Jolis, E. M.; et al. The Recycling of End-of-Life Lithium-Ion Batteries and the Phase Characterisation of Black Mass. *Recycling* **2023**, *8* (4), 59.

(5) Kim, S.; Bang, J.; Yoo, J.; Shin, Y.; Bae, J.; Jeong, J.; Kim, K.; Dong, P.; Kwon, K. A Comprehensive Review on the Pretreatment Process in Lithium-Ion Battery Recycling. *J. Clean. Prod.* **2021**, *294*, 126329.

(6) Wang, Q.; Sun, J.; Chen, C. Thermal Stability of LiPF6/EC + DMC + EMC Electrolyte for Lithium-Ion Batteries. *Rare Met.* **2006**, *25*, 94−99.

(7) Costa, C. M.; Lanceros-Méndez, S. Recent Advances on Battery Separators Based on Poly(Vinylidene Fluoride) and Its Copolymers for Lithium-Ion Battery Applications. *Curr. Opin. Electrochem.* **2021**, *29*, 100752.

(8) Arshad, F.; Li, L.; Amin, K.; Fan, E.; Manurkar, N.; Ahmad, A.; Yang, J.; Wu, F.; Chen, R. A Comprehensive Review of the Advancement in Recycling the Anode and Electrolyte from Spent Lithium Ion Batteries. *ACS Sustainable Chem. Eng.* **2020**, *8* (36), 13527−13554.

(9) Li, S. Y.; Ma, P. H.; Cui, X. L.; Ren, Q. D.; Li, F. Q. Studies on the Thermal Decomposition Kinetics of LiPF6 and LiBC4O8. *J. Chem. Sci.* **2008**, *120*, 289−292.

(10) Lekgoathi, M.; Vilakazi, B.; Wagener, J. Decomposition Kinetics of Anhydrous and Moisture-Exposed LiPF6 Salts by Thermogravimetry. *J. Fluorine Chem.* **2013**, *149*, 53.

(11) Kock, L. D.; Lekgoathi, M. D. S.; Crouse, P. L. Solid-State Vibrational Spectroscopy of Anhydrous Lithium Hexafluorophosphate (LiPF6). *J. Mol. Struct.* **2012**, *1029*, 145.

(12) Wang, M.; Tan, Q.; Liu, L.; Li, J. A Facile, Environmentally Friendly, and Low-Temperature Approach for Decomposition of Polyvinylidene Fluoride from the Cathode Electrode of Spent

Lithium-Ion Batteries. *ACS Sustainable Chem. Eng.* **2019**, *7*, 12799−12806.
(13) Hirschler, M. Effect of Oxygen on the Thermal Decomposition of Poly(Vinylidene Fluoride). *Eur. Polym. J.* **1982**, *18* (5), 463−467.
(14) Danz, P.; Aryan, V.; Möhle, E.; Nowara, N. Experimental Study on Fluorine Release from Photovoltaic Backsheet Materials Containing PVF and PVDF during Pyrolysis and Incineration in a Technical Lab-Scale Reactor at Various Temperatures. *Toxics* **2019**, *7* (3), 47.
(15) Knight, G. J.; Wright, W. W. The Thermal Degradation of Hydrofluoro Polymers. *J. Appl. Polym. Sci.* **1972**, *16* (3), 683−693.
(16) Tanaka, F.; Gungaajav, L.; Terakado, O.; Kuzuhara, S.; Kasuya, R. Dehydrofluorination Behavior of Poly(Vinylidene Fluoride) during Thermal Treatment Using Calcium Carbonate. *Thermochim. Acta* **2021**, *702*, 178977.
(17) Hoq, M.; Jang, D.; Rahman, M.; Yep, J.; Kim, J.-H.; Shin, H. Efficient Direct Cathode Regeneration for Spent Lithium-Ion Batteries via Planetary Centrifugal Mixing and Eutectic Salts. *ACS Sustainable Chem. Eng.* **2025**, *13* (37), 15269−15279.
(18) Wang, W.; Zhang, Y.; Liu, X.; Xu, S. A Simplified Process for Recovery of Li and Co from Spent LiCoO2 Cathode Using Al Foil as the In-Situ Reductant. *ACS Sustainable Chem. Eng.* **2019**, *7*, 12222−10364.
(19) Nababan, D. C.; Mukhlis, R.; Durandet, Y.; Prentice, L. H.; Rhamdhani, M. A. Separation of Li and Co from LiCoO2 Cathode Material through Aluminothermic Reduction: Investigation of the Thermite Reaction. *Metall. Mater. Trans. B* **2024**, *55*, 905−924.
(20) Ahn, Y.; Koo, W.; Yoo, K.; Alorro, R. D. Carbothermic Reduction Roasting of Cathode Active Materials Using Activated Carbon and Graphite to Enhance the Sulfuric Acid-Leaching Efficiency of Nickel and Cobalt. *Minerals* **2022**, *12* (8), 1021.
(21) Babanejad, S.; Ahmed, H.; Andersson, C.; Samuelsson, C.; Lennartsson, A.; Hall, B.; Arnerlöf, L. High-Temperature Behavior of Spent Li-Ion Battery Black Mass in Inert Atmosphere. *J. Sustain. Metall.* **2022**, *8*, 566−581.
(22) Liu, P.; Xiao, L.; Tang, Y.; Chen, Y.; Ye, L.; Zhu, Y. Study on the Reduction Roasting of Spent LiNixCoyMnzO2 Lithium-Ion Battery Cathode Materials. *J. Therm. Anal. Calorim.* **2019**, *136*, 1323−1332.
(23) Liu, P.; Xiao, L.; Chen, Y.; Tang, Y.; Wu, J.; Chen, H. Recovering Valuable Metals from LiNixCoyMn1−x−yO2 Cathode Materials of Spent Lithium-Ion Batteries via a Combination of Reduction Roasting and Stepwise Leaching. *J. Alloys Compd.* **2019**, *783*, 743−752.
(24) Pan, C.; Shen, Y. Pyrometallurgical Recycling of Spent Lithium-Ion Batteries from Conventional Roasting to Synergistic Pyrolysis with Organic Wastes. *J. Energy Chem.* **2023**, *85*, 547−561.
(25) Willard, H. H.; Winter, O. B. Volumetric Method for Determination of Fluorine. *Ind. Eng. Chem. Anal. Ed.* **1933**, *5* (1), 7−10.
(26) Grazulis, S.; Daskevic, A.; Merkys, A.; Chateigner, D.; Lutterotti, L.; Quirós, M.; Serebryanaya, N. R.; Moeck, P.; Downs, R. T.; Le Bail, A. Crystallography Open Database (COD): An Open-Access Collection of Crystal Structures and Platform for World-Wide Collaboration. *Nucleic Acids Res.* **2012**, *40* (D1), D420−D427.
(27) Bale, C.; Bélisle, E.; Chartrand, P.; Decterov, S.; Eriksson, G.; Gheribi, A.; Hack, K.; Jung, I.-H.; Kang, Y.-B.; Melançon, J.; Pelton, A.; Petersen, S.; Robelin, C.; Sangster, J.; Spencer, P.; Van Ende, M.-A. FactSage Thermochemical Software and Databases, 2010−2016. *Calphad* **2016**, *55*, 1−19.
(28) Jribi, S.; Miyazaki, T.; Saha, B. B.; Pal, A.; Younes, M. M.; Koyama, S.; Maalej, A. Equilibrium and Kinetics of CO2 Adsorption onto Activated Carbon. *Int. J. Heat Mass Transfer* **2017**, *108*, 1941−1946.
(29) Fernandes, Y.; Bry, A.; De Persis, S. Thermal Degradation Analyses of Carbonate Solvents Used in Li-Ion Batteries. *J. Power Sources* **2019**, *414*, 250−261.
(30) Leanza, D.; Mirolo, M.; Vaz, C. A. F.; Novák, P.; El Kazzi, M. Surface Degradation and Chemical Electrolyte Oxidation Induced by the Oxygen Released from Layered Oxide Cathodes in Li-Ion Batteries. *Batteries Supercaps* **2019**, *2*, 482−492.
(31) Bak, S. M.; Hu, E.; Zhou, Y.; Yu, X.; Senanayake, S. D.; Cho, S. J.; Kim, K. B.; Chung, K. Y.; Yang, X. Q.; Nam, K. W. Structural Changes and Thermal Stability of Charged LiNixMnyCozO2 Cathode Materials Studied by Combined *In Situ* Time-Resolved XRD and Mass Spectroscopy. *ACS Appl. Mater. Interfaces* **2014**, *6* (22), 22594−22601.
(32) Hu, E.; Bak, S. M.; Zhou, Y.; Yu, X.; Senanayake, S. D.; Cho, S. J.; Kim, K. B.; Chung, K. Y.; Yang, X. Q.; Nam, K. W. Structural Changes and Thermal Stability of Charged LiNixMnyCozO2 Cathode Materials Studied by Combined *In Situ* Time-Resolved XRD and Mass Spectroscopy. *ACS Appl. Mater. Interfaces* **2014**, *6* (22), 22594−22601.
(33) Jung, R.; Strobl, P.; Maglia, F.; Stinner, C.; Gasteiger, H. A. Temperature Dependence of Oxygen Release from LiNi0.6Mn0.2-Co0.2O2 (NMC622) Cathode Materials for Li-Ion Batteries. *J. Electrochem. Soc.* **2018**, *165* (11), A2869−A2879.
(34) Wang, T.; Ren, K.; Xiao, W.; Dong, W.; Qiao, H.; Duan, A.; Pan, H.; Yang, Y.; Wang, H. Tuning the Li/Ni Disorder of the NMC811 Cathode by Thermally Driven Competition between Lattice Ordering and Structure Decomposition. *J. Phys. Chem. C* **2020**, *124* (9), 5600−5607.
(35) Windisch-Kern, S.; Holzer, A.; Wiszniewski, L.; Raupenstrauch, H. Investigation of Potential Recovery Rates of Nickel, Manganese, Cobalt, and Particularly Lithium from NMC-Type Cathode Materials (LiNixMnyCozO2) by Carbo-Thermal Reduction in an Inductively Heated Carbon Bed Reactor. *Metals* **2021**, *11*, 1844.
(36) Rashed, A. H.; Rao, Y. K. Kinetics of Reduction of Nickel Oxide with Hydrogen Gas in the 230−452 °C Range. *Chem. Eng. Commun.* **1997**, *156* (1), 1−30.
(37) Bhandari, G. S.; Dhawan, N. Gaseous Reduction of NMC-Type Cathode Materials Using Hydrogen for Metal Recovery. *Process Saf. Environ. Prot.* **2023**, *172*, 523−534.
(38) Huang, Z.; Yu, D.; Makuza, B.; Tian, Q.; Guo, X.; Zhang, K. Hydrogen Reduction of Spent Lithium-Ion Battery Cathode Material for Metal Recovery: Mechanism and Kinetics. *Front. Chem.* **2022**, *10*, 1019493.
(39) Zhang, H.; Tang, A.; Luo, F.; Xie, X.; Yang, L.; Zheng, Y.; Tao, X.; Qiu, C.; Wang, C.; Peng, A.; Luo, X.; Shao, P. Extraction of Valuable Metals from Spent Cathode Materials by Reductive Roasting in Methane Atmosphere. *Sep. Purif. Technol.* **2023**, *318*, 123995.
(40) Kharatyan, S. L.; Chatilyan, H. A.; Manukyan, K. V. Kinetics and Mechanism of Nickel Oxide Reduction by Methane. *J. Phys. Chem. C* **2019**, *123* (35), 21513−21521.
(41) Vardanyan, E. A.; Asaturyan, S. G.; Simonyan, A. R.; Avagyan, H. H.; Kharatyan, S. L.; Manukyan, K. V. Initial Stages of Hydrogen-Enhanced Methane Reduction of Nickel Oxide. *Ind. Eng. Chem. Res.* **2024**, *63* (10), 4264−4274.
(42) Fujiwara, K.; Ito, K.; Kuzuhara, S.; Terakado, O.; Hosoya, N.; Hayashi, H.; Kasuya, R. Development of Fluorine Fixation Processes for the Horizontal Recycling of Lithium. *Materials* **2025**, *18* (9), 2050.
(43) Zhao, Y.; Wen, Y.; Yang, Y.; Xu, S. Recovery of Fluorine-Containing Resources from Spent Lithium-Ion Batteries as High-Value Products. *Resour. Conserv. Recycl.* **2025**, *221*, 108403.

https://doi.org/10.1021/acssuschemeng.5c10344
ACS Sustainable Chem. Eng. XXXX, XXX, XXX−XXX